Zirconolite and Murataite for the Immobilization of Actinides

Subjects: Chemistry, Inorganic & Nuclear

Contributor: Sergey V. Yudintsev, Maximilian S. Nickolsky, Michael I. Ojovan, Olga I. Stefanovsky, Boris S. Nikonov, Amina S. Ulanova

Zirconolite is highly stable in nature, with isotope systems that have been closed for hundreds of million years, making it possible for age determination. Murataite is a very rare mineral, its synthetic counerpart was first discovered in the Synroc matrix from defense waste obtained by sintering. Synthetic zirconolie and murataite can be applied for nuclear waste immobilization.

Keywords: actinides ; immobilisation ; matrix ; zirconolite ; polytype ; murataite

1. Introduction

The development of sustainable nuclear power generation independent of uranium resources involves the reprocessing of spent nuclear fuel (SNF) with the recycling of uranium and actinides (Pu). The PUREX extraction process is industrially used for this, having initially been developed about 70 years ago in the USA to extract Pu and U for military purposes. Reprocessing a tonne of SNF generates 13–31 m^3 of liquid high-level radioactive waste (HLW). HLW can contain stable and radioactive isotopes of fission products (Cs, Ba, I, Sr, REE, Mo, Zr, Tc, Ru, Rh, Pd), residual U and Pu, minor actinides (Np, Am, Cm), corrosion products (Zr, Ni, Cr, Mn, Fe, Co, Al), and technological impurities (Na, Fe, Al, S). Liquid HLW poses an environmental hazard and must be converted into a stable form for placement in a deep underground repository. Since 1978, HLW has been immobilised in B–Si glass (France, UK, USA, Belgium, etc.), and since 1987, in Al–P glass (Russia). About 30 thousand tonnes of borosilicate and almost 7 thousand tonnes of aluminophosphate vitrified HLW have been produced up to now, and this process continues. Significant volumes of solid and liquid HLW are stored at radiochemical plants in the USA and Russia.

The weak point of glass is the low HLW loading, which is 3–5 wt.% for Al–P and 15–20 wt.% for B–Si matrices, as up to 1.8 t (0.6 m^3) Al–P and 0.4 t (0.15 m^3) B–Si glass matrix is produced on processing of 1 t of spent nuclear fuel. This reduces the efficiency of underground disposal, including the search for locations and the construction process, which require considerable time and resources. Other drawbacks of glass includes potential decrease in retaining properties due to crystallization, and on contact with water the formation of radioactive colloids migrating in the geological environment. The problems of HLW management can be more effectively solved by partitioning HLW into groups of elements with similar properties, for their immobilization in optimal matrices. One of these groups is the fraction containing rare earth elements (REE) and minor actinides (MA) such as Am and Cm.

Russia is implementing a strategy of two-component nuclear power generation, with slow and fast neutron reactors operating in a closed nuclear fuel cycle [1]. This will reduce the need for uranium through the recycling of actinides, and will allow the extraction of useful stable and radioactive isotopes necessary for industry. The reprocessing of SNF will result in the generation of liquid high-level radioactive waste, so the development of methods for HLW optimal management is highly urgent. The greatest ecological concern is caused by long-lived actinides (Np, Pu, Am, Cm) and their daughter products [2][3][4], in particular, ^{241}Am ($T_{½}$ = 432 years) decays to form ^{237}Np with a half-life of 2.1 million years.

In the advanced nuclear fuel cycle, MAs are extracted for transmutation in fast reactors in homogeneous (Np) and heterogeneous (Am) modes [1][4][5][6][7]. There is a proposal to store Curium for 70 to 200 years, to decay into Pu and fabricate nuclear fuel. Depending on the degree of actinide extraction, the radioactive waste hazard will be equal to the value for uranium ore in 300, 500, or 10,000 years [1][2][4][7][8][9]. This concept is known as “radiative equivalence”. In a shorter time, about 100 years, radiological (oncological) equivalence between them will occur [10]. The application of this approach requires the creation of sophisticated technologies for processing SNF and extracting transplutonium elements (TPE) from HLW. Methods for partitioning REE, americium, and curium with similar properties, the separation of Am and Cm, fabrication of fuel with Np and Am, and its processing after irradiation in a fast reactor are still far from being

implemented [11][12][13][14]. The timing of closing the nuclear fuel cycle, involving the partitioning of minor actinides (Np, Am, Cm), fuel fabrication, its irradiation in fast reactors, and subsequent reprocessing, has been shifted to 2050 [15], which is more than 30 years longer than previous estimates.

Comparison of the potential harm to human health from radioactive waste and U ore (radiative and oncological equivalence) is based on the assumption of their complete dissolution in groundwater. However, there are no real grounds for this, since uranium deposits with an age of many millions of years are known, representing reserves of hundreds of thousands of tonnes at concentrations of up to 20 wt.%. Reliably established reserves of uranium in these deposits are approach six million tones, and estimated resources are 7.5 million tonnes. The number of known U deposits exceeds 1800, the oldest of which are over 2 billion years old [16][17][18]. Since the solubilities of HLW and uranium ores in groundwater are very low, it makes no sense to compare their hazards. Environmental hazard assessment through the volume of water required to dissolve elements to a safe level has shown that Hg, Se, Pb, Cd, and As ores containing the first wt.% of these elements pose an even greater environmental threat [19][20][21]. Unlike radionuclides, which gradually decrease in quantity due to decay, the danger from these toxic elements does not decrease with time.

2. Zirconolite and Murataite as Matrices for the Immobilization of Actinides

The choice of actinide matrix is largely determined by crystal–chemical parameters. At high temperatures, the most common oxidation states of actinides are $Pu^{3+/4+}$, $(Am, Cm)^{3+}$ and Np^{4+} [22]. REE elements of the REE-MA fraction (MA = Am, Cm) exist as trivalent ions, Ce can be partially in the form of Ce^{4+}. To simulate actinides in matrices, lanthanides are used, and Ce, Th or U are introduced instead of Pu [23][24][25]. Due to close ionic radii [26], Ce^{3+} simulates Pu^{3+}, while Nd^{3+} and Eu^{3+} simulate Cm^{3+} and Am^{3+}. Monovalent Th^{4+} and Hf^{4+} are sometimes used to replace Np and Pu. Particular attention is paid here to studies using Nd, Sm, or La, which dominate among the REE fission products of SNF and in the composition of the REE-MA fraction of HLW. The average ionic radius of the REE–MA fraction is 1.11 Å, the same as for Nd^{3+}, larger than that of Sm^{3+} (1.08 Å), but smaller than that of La^{3+} (1.16 Å). Therefore, Nd is the best simulant of the REE-MA fraction when studying the structure and waste loading of the matrices, the distribution of elements between phases, stability in water, and their main physical properties; density, heat capacity, thermal conductivity, and mechanical durability, which weakly depend on whether the simulant element is radioactive.

For the immobilization of actinide containing nuclear waste, crystalline zirconolite and glass-crystalline materials with zirconolite have been proposed. They may be obtained by all known methods—sintering at atmospheric or elevated pressures, melting and crystallization, high-speed pulsed electric current sintering, and self-propagating high-temperature synthesis [27][28][29][30][31][32][33][34][35][36][37][38][39][40][41][42][43][44][45][46][47][48]. Zirconolite is stable in various natural conditions [31][49][50][51]; natural zirconolite is a rare mineral of terrestrial and lunar igneous rocks, and metasomatites. In nature, zirconolites from different localities have been found to contain UO_2, ThO_2, or REE_2O_3 reaching 24, 22, or 32 wt%, respectively [51][52][53]. Due to the high conent of U and Th, zirconolite is often amorphous; this occurs at irradiation doses above 5×10^{18} α-decays/g [49]. In **Figure 1**, three minerals can be distinguished by composition: Zirconolite, monoclinic (polytype 2M), polymignite, orthorhombic (3O), zirkelite, hexagonal (3T) [54].

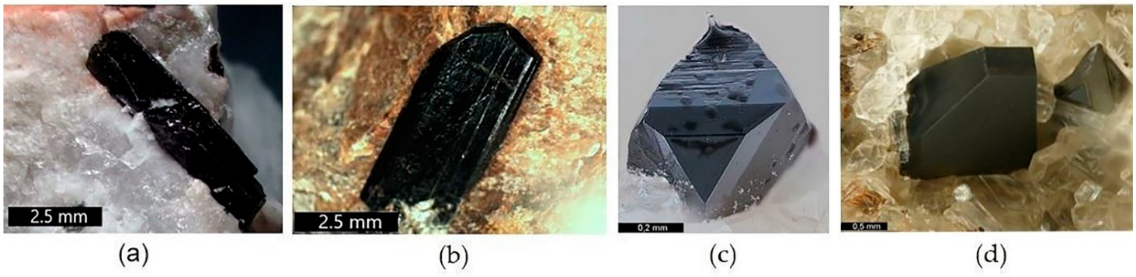

Figure 1. Natural zirconolites: (**a**,**b**) 3O (Vestfold og Telemark, Norway); and (**c**,**d**) 3T (Eifel Volcanic Fields, Germany; Fogo Volcano, Portugal).

The above noted classification was approved by the Commission on New Minerals of the International Mineralogical Association [55]; hence, polymignite and zirkelite are no longer used. The 2M polytype is common in carbonatites, while the 3O and 3T polytypes are common in volcanics and metasomatites [56][57] with a content of REE^{3+}, Th, Fe, and Nb.

Artificial zirconolite was observed for the first time in Synroc polyphase ceramics [28], an alternative to B–Si glass for HLW immobilization. In the first version, Synroc A, the $(Zr,Ca,Ti)O_2$ oxide initially was determined, but X-ray microanalysis found that its formula corresponded to $CaZrTi_2O_7$ with an admixture of Al for charge balance when the Ca/Zr ratio varied. This allowed attribution of the phase found to an artificial analog of the mineral zirconolite, which later was confirmed by the X-

ray diffraction data. In the all Synroc-type ceramics (B, C, D, E, F), zirconolite is the main host for actinides and REE [28][29][58][59][60]. It forms five polytypes—2M, 4M, 3O, 3T, and 6T, the figure is the number of layers of TiO_6 octahedra, the letter is the symmetry of the lattice. The structure of the 2M polytype consists of trigonal and hexagonal rings of Ti-O octahedra, some of the Ti atoms are surrounded by 5 O^{2-} anions. These correspond to three positions of Ti atoms: Ti(1) and Ti(3) with a coordination number (cn) equal to VI (octahedrons), and Ti(2) with cn = V (bipyramids). The unit cell of zirconolite contains eight Ti(1) atoms, and four each of Ti(3) and Ti(2) atoms. Ca^{2+} (cn = VIII) and Zr^{4+} (cn = VII) are located between two networks of TiO_6 octahedra. One structural module is formed by a pair of layers of TiO_6 octahedra with interlayer cations. Its rotation through an angle multiple of 120° forms a cell of zirconolites 3T and 3O. With a change in the stacking sequence of Ca/Zr and Ti–O layers, other polytypes arise, and the structure of zirconolite 4M is a four-layer package of sheets of zirconolite 2M and pyrochlore (**Figure 2**).

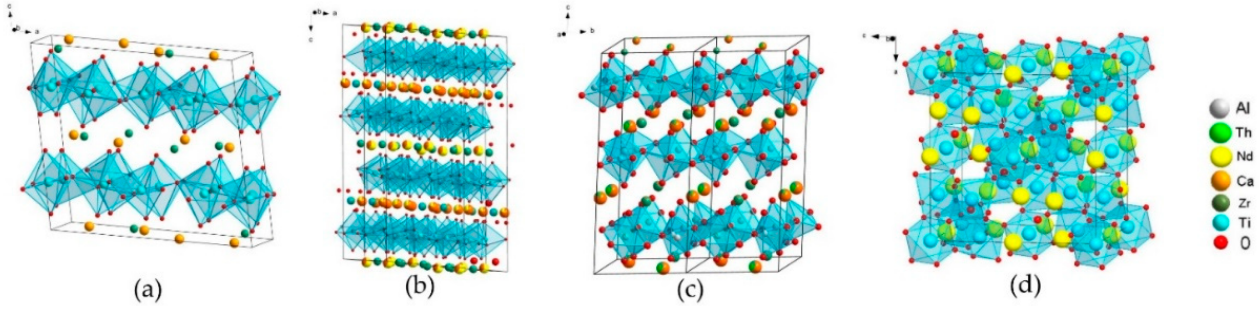

Figure 2. Structure of zirconolite polytypes (**a**) 2M, (**b**) 4M, (**c**) 3T, (**d**) pyrochlore $Nd_2(Ti,Zr)_2O_7$.

The result is a doubling of the cell parameter along the *c* axis with preservation of monoclinic symmetry [61]. Variations in composition of the 2M phase are described by the formula $CaZr_xTi_{3-x}O_7$, "x" = 0.83–1.33. The replacement of Zr by Hf retains the 2M structure in $CaHfTi_2O_7$ and $Ca_{1-x}Nd_xHfTi_{2-x}Al_xO_7$ (x = 0.01, 0.2) [62], which is due to the closeness of ionic radii of Zr^{4+} (0.78 Å) and Hf^{4+} (0.76 Å) (cn = VII).

Among the first works to note the effect of zirconolite composition on its structure were articles [30][59][63][64]. A description of all five zirconolite polytypes known so far is given in [65]. Their formation depends on the type of substitutions, charge and radius of cations, temperature, and oxidizing conditions [66]. Polytypes 2M and 4M are monoclinic (sp. gr. *C2/c*), 3O is orthorhombic (*Acam*), and 3T and 6T are hexagonal ($P3_121$). The most common polytypes in actinide matrices are 2M and 4M [66], less common are 3O [38] and 3T [24][67], there are no data for the 6T polytype. For phases of composition $(Ca_{1-x}{}^{239}Pu_x)Zr\ (Ti_{2-2x}Fe_{2x})O_7$ (x = 0.1–0.7), the 2M polytype is stable up to "x" = 0.3, and 3T appears at "x" = 0.3 and 0.4. Replacing Pu with Ce increases the field of stability of the 2M polytype. Zirconolite 3T is often formed using thorium as a simulator. A reducing medium (5% H_2/N_2) is favorable for the formation of 3T zirconolite $CaZr_{1-x}Th_xTi_2O_7$ at x ≥ 0.20 [66], $Ca_{0.8}Ti_{1.35}Zr_{1.3}Th_{0.15}Al_{0.4}O_7$ crystallizes in the same 3T type [68]. Fine intergrowth of 2M and 3T polytypes was established in glass ceramics obtained in the SiO_2–Al_2O_3–CaO–ZrO_2–TiO_2–ThO_2 system [36].

$CaZr_{1-x}(Ce/U/Th/Pu)_{4+x}Ti_2O_7$ (x = 0.1–0.6) phases are represented by zirconolite 2M, 4M and/or pyrochlore (**Table 1**), and their structures shown in **Figure 2**, with data from [66].

Table 1. Phases in samples of bulk composition $CaZr_{1-x}(Ce/U/Th/Pu)_{4+x}Ti_2O_7$ at "x" from 0.1 to 0.6.

Cation	x = 0.10	x = 0.20	x = 0.30	x = 0.40	x = 0.50	x = 0.60
Ce^{4+}	2M	2M + 4M	2M + 4M	2M + 4M	2M + 4M + P	4M + P
U^{4+}	2M	2M + 4M	2M + 4M	4M + P	4M + P	4M + P
Th^{4+}	2M + P	2M + P	2M + P	2M + P	2M + P	P
Pu^{4+}	2M	2M + 4M	2M + 4M	4M + P	4M + P	P

2M, 4M—zirconolite polytypes, P—pyrochlore.

Information about zirconolite polytypes in glass ceramics is controversial. On the one hand [44][45], in B–Si glass ceramics, with an increase in the contents of CeO_2 and Nd_2O_3 up to 15 wt%, transition of 2M polytype into 4M was observed. However, when studying glass ceramics with $Ca_{1-x}Zr_{1-x}Nd_{2x}Ti_2O_7$, $Ca_{1-x}Nd_xZrTi_{2-x}Al_xO_7$, and $CaZr_{1-x}Ce_xTi_2O_7$ (x = 0–0.5) phases, no transition of the 2M to 4M polytype was observed, in contrast to ceramics of the same composition [69]. In glass ceramics with REE and actinides, the 2M polytype is more stable due to the limited solubility of tri- and, especially,

tetra-valent cations in the original glass [70][71] and low distribution coefficients of Nd^{3+}, Ce^{3+}, Th^{4+} between zirconolite and glass [36][72][73] during crystallization in the glass ceramic.

Compositions of natural and artificial zirconolite can be affected by substitutions [31][52][59], the main ones being $(Ce,An)^{4+} \rightarrow Zr^{4+}$; $2(Ln,An)^{3+} \rightarrow Ca^{2+} + Zr^{4+}$; $(Ln,An)^{3+} + (Al,Fe)^{3+} \rightarrow Ca^{2+} + Ti^{4+}$; and more rarely: $An^{4+} + (Fe,Co)^{2+} \rightarrow Ca^{2+} + Ti^{4+}$; $(Ce,An^{4+}) + 2(Al,Fe,Cr)^{3+} \rightarrow Ca^{2+} + 2Ti^{4+}$ (Ln are lanthanides, An are actinides). The replacement of 2M zirconolite by more complex 4M, 3O, or 3T polytypes has been observed with an increase in the concentration of tri- (La, Ce, Nd, Dy, Y, Am, Cm) and tetravalent ions (Ce, U, Np, Pu), replacing Ca^{2+} and Zr^{4+} [66][74][75][76][77]. An increase in the content of Nd^{3+} or $(Ce/U/Th/Pu)^{4+}$ in the samples resulted in the zirconolite sequence structure 2M—3T—4M—pyrochlore [62][66].

In many early [28][29][58][60][78][79] and more recent [48][80][81] studies of matrices, the zirconolite polytype was not specified. There are several explanations for this and the first is that the similarity of properties [36] may make it unnecessary to identify the exact zirconolite polytype. There is no clear evidence that structural features somehow affect the resistance of zirconolite to radiation or corrosion in water [74]. It can only be argued that the polytypes have different capacities with respect to the actinide and REE-actinide fractions, i.e., maximum value for 4M, minimum for 2M, and intermediate for zirconolite 3O or 3T. With an actinide and REE content of up to 0.20–0.25 atoms, the zirconolite polytype 2M is stable [82][83]. The boundary between 2M and 4M polytypes for the $Ca_{1-x}Zr_{1-x}Sm_{2x}Ti_2O_7$ solid solution passes at x = 0.35 [84].

Artificial zirconolite with REE and Pu is stable in alkaline and acidic solutions up to 500°C at 50 MPa, even after amorphization of the crystalline lattice [33][39][52][85][86][87][88].

Murataite was first discovered in the Synroc matrix from defense waste obtained by sintering [89]. In the sample from the HLW simulator [90][91][92], obtained by melting and crystallization, it was formed from the melt last, growing on zirconolite grains (**Figure 3**) [93].

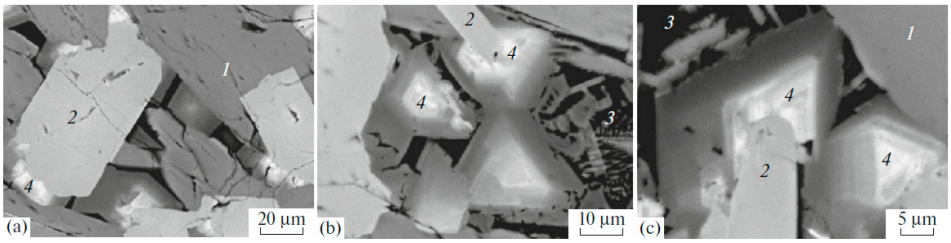

Figure 3. SEM images of the melted Synroc-type ceramic with model nuclear wastes: (1) hollandite, (2) zirconolite, (3) rutile and glass, (4) zoned murataite crystals overgrown on the zirconolite grains. (**a**) general view; (**b**,**c**) details with murataite–zirconolite intergrowths.

Such a close relationship between these two phases is due to the affinity of the structures both derived from the fluorite-type lattice. Murataite is this optimal host phase for tetravalent actinides (Th, U, Np, Pu); in this case it dominates in the matrix (**Figure 4**) [90][91].

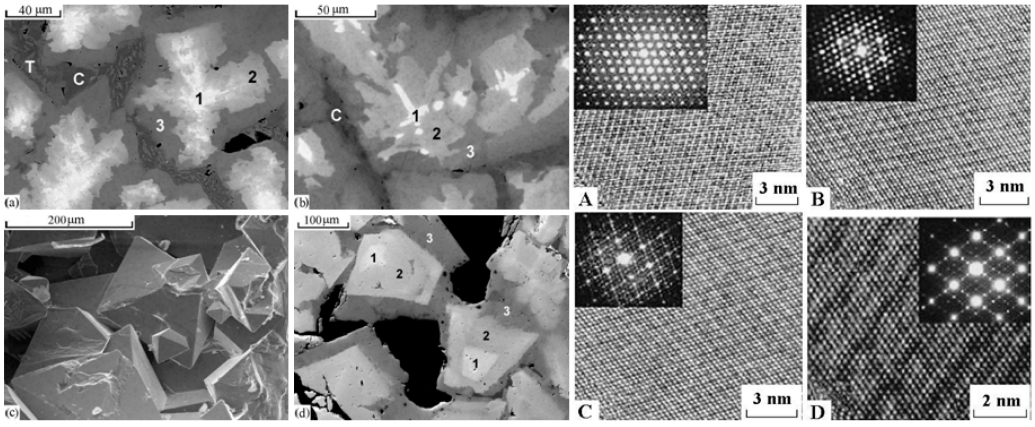

Figure 4. Left: SEM images of ceramics with 10% (**a**) UO_2, (**b**) PuO_2, (**c**,**d**) ThO_2. (1) murataite 5C, (2) murataite 8C, (3) murataite 3C, (C) crichtonite, (T) pyrophanite; pores are black. Right: HRTEM micrographs of (**A**) pyrochlore, murataite (**B**) 3C, (**C**) 5C, (**D**) 8C taken with a high-resolution transmission electron microscope. Inserts: SAED patterns. Lines are atomic layers.

In the nature, murataite has been found in only two locations, making it significantly rarer than zirconolite. Unlike zirconolite, murataite contains neither U nor Th, and of the rare earth elements contains only Y.

With an increase in the content of trivalent REE in the sample, perovskite-like phase has been observed, a less stable phase at elevated water solution temperatures, especially above 100 °C [94]. Synthetic murataites occur as phases 3C, 5C, 7C, and 8C (the number is the multiplicity of the cell parameter relative to the fluorite cell, C is the cubic symmetry of the lattice). They constitute the polysomatic series murataite 3 C—pyrochlore [95][96][97][98].

Murataites 5C and 8C are the most common in samples, whereas 3C is less common and 7C is very rare. All of them crystallize in the sp. gr. F-43m, so their X-ray diffraction patterns are similar. In melted ceramics, murataite forms zoned crystals with pyrochlore or murataite 5C at the center, and murataite 8C or 3C towards the edges (**Figure 4**). In samples obtained by sintering, murataite 5C and murataite 8C formed separate grains [99]. The pyrochlore module is responsible for actinide content, and the murataite block is responsible for corrosion products (Fe, Al, Mn). Although the concentrations of actinides decrease in the order pyrochlore–murataite 5C–8C–3C, while Fe and Al increase, the assignment of the phase to a specific polysome only by its composition may be incorrect.

Elucidation of the polytype (polysome) of phase requires examination by X-ray phase analysis with attention to weak reflections from a certain range of angles, or in a transmission electron microscope [38][62][65]. This problem is often complicated by the multiphase composition of matrices and the presence of several phases with similar structures—zirconolite, pyrochlore, and murataite. For simultaneous study of the composition and structure of phases, a combination of scanning electron microscopy (SEM) and electron backscatter diffraction (EBSD) can be applied [100][101]. The possibilities of this approach will later be shown using the example of samples containing zirconolite and murataite, but first brief information about the electron backscatter diffraction method must be presented.

Conclusions: Morphotropic transitions in matrices of actinides composed of phosphates, titanates and zirconates of rare earth elements resulted in a variety of structures of the host phases. They also exhibit polytypism (zirconolite) and polysomatism (pyrochlore – murataite se-ries). One of the important requirements for the matrix is a high waste content; therefore, the 4M, 3T, and 3O zirconolite polytypes and the 5C and 8C murataite polysomes are of interest. Their diagnostics by X-ray phase analysis is often difficult due to the multiphase structure of matrices, the presence of several phases at once with a structure derived from the fluorite lattice (pyrochlore, zirconolite, murataite, cubic Zr oxide). The structure types of phases in samples with simulators of actinide and REE-actinide fractions (Th, Nd) was determined by the electron backscatter diffraction.

The purpose of this research is to study the structure of zirconolite and murataite in two matrices with actinides simulators (Th, Nd) obtained by melting in air at 1500 °C in glassy carbon crucibles. The sample with Th contains three phases: zirconolite-3T of composition $Ca_{0.67}Th_{0.19}Ti_{1.84}Zr_{0.89}Fe_{0.07}Mn_{0.21}Al_{0.13}O_7$ and two polysomes of murataite 8C (predominated) with formula calculated from their chemical composition: $Ca_{76.52}Th_{19.4}Ti_{254.73}Zr_{37.86}Fe_{14.54}Mn_{50.35}Al_{33.55}O_{823}$ and $Ca_{65.04}Th_{9.53}Ti_{259.29}Zr_{6.31}Fe_{34.68}Mn_{58.8}Al_{65.04}O_{823}$. The zirconolite in the sample with Nd is rep-resented by the 4M polytype, and there is also pyrochlore. The stability fields of zirconolite polytypes depend on the size of the cations that replace the main elements (Ca^{2+}, Ti^{4+}, and Zr^{4+}). The replacement of Zr^{4+} by $(Ce, U, Pu)^{4+}$ causes the transformation of the 2M polytype into 4M; replacements of $Ca^{2+} – Zr^{4+}$ and $Ca^{2+} – Ti^{4+}$ with $Pu^{3+/4+}$, REE^{3+}, and small ions $(Al, Cr, Fe, Ti)^{3+}$ stabilize polytypes 3O and 3T. Researchers note the important role of pyrochlore in the structures of the 4M zirconolite polytype and the 8C polysome of murataite, which once again confirms close relationship between the structures of these phases. In general, the EBSD is an effective method for diagnosing polytypes and members of polysomatic series in HLW crystalline matrices.

References

1. Adamov, E.O.; Mochalov, Y.S.; Rachkov, V.I.; Khomyakov, Y.S.; Shadrin, A.Y.; Kascheev, V.A.; Khaperskaya, A.V. Spent nuclear fuel reprocessing and nuclear materials recycling in two-component nuclear energy. At. Energy 2021, 130, 29–35.
2. Implications of Partitioning and Transmutation in Radioactive Waste Management; Technical Reports Series, No. 435; I AEA: Vienna, Austria, 2004; 127p.
3. Westlen, D. Reducing radiotoxiciti in the long run. Progr. Nucl. Energy 2007, 49, 597–605.

4. Potential Benefits and Impacts of Advanced Nuclear Nuclear Fuel Cycles with Actinide Partitioning and Transmutation; Rep. 6894; NEA OECD: Paris, France, 2011; 73p.
5. Berthou, V.; Degueldre, C.; Magill, J. Transmutation characteristics in thermal and fast neutron spectra: Application to a mericium. J. Nucl. Mater. 2003, 320, 156–162.
6. Fuels and Materials for Transmutation; Rep. 5419; NEA OECD: Paris, France, 2005; 239p.
7. Salvatores, M.; Palmiotti, G. Radioactive waste partitioning and transmutation within advanced fuel cycles: Achievemen ts and challenges. Progr. Partickle Nucl. Phys. 2011, 66, 144–166.
8. Adamov, E.O.; Lopatkin, A.V.; Muravyov, E.V.; Rachkov, V.I.; Khomyakov, Y.u.S. National strategy for the development of nuclear energy: Two approaches to a new technological platform for nuclear energy. Izv. RAN Energy 2019, 3–14. (I n Russian)
9. Lopatkin, A.V.; Platonov, I.V.; Popov, V.E. Conditions for reaching radiation equivalence of native raw materials and lon g-lived radioactive waste in nuclear energy in Russia. At. Energy 2021, 129, 188–193.
10. Ivanov, V.K.; Chekin SYu Menyailo, A.N.; Maksyutov, M.A.; Tumanov, K.A.; Kashcheeva, P.V.; Lovachev, S.S.; Spirin, E. V.; Solomatin, V.M. Radiotoxicity of long-lived high-level waste from fast reactors in scenarios for handling irradiated nu clear fuel to achieve radiation and radiological equivalence with natural uranium. Radiat. Risk 2019, 28, 8–24. (In Russi an)
11. Spent Nuclear Fuel Reprocessing Flowsheet; NEA OECD: Paris, France, 2012; 120p.
12. State-of-the-Art Report on the Progress of Nuclear Fuel CYCLE Chemistry; NEA: Paris, France, 2018; 299p.
13. Skupov, M.V.; Glushenkov, A.E.; Tarasov, B.A.; Abramov, S.V.; Kuzin, M.A.; Nikitin, O.N.; Zabudko, L.M.; Grachev, A.F.; Zherebtsov, A.A.; Mochalov, Y.S. Development of Technologies for Production of Fuel with Minor Actinides. Nucl. Engin. Des. 2021, 382, 111379.
14. Kuzin, M.A.; Abramov, S.V.; Grachev, A.F.; Zherebtsov, A.A.; Zabudko, L.M.; Nikitin, O.N.; Kuzmin, S.V. Production and study of tablets of mixed nitrides of uranium, plutonium, americium and neptunium. Chem. Technol. 2021, 22, 36–43. (I n Russian)
15. NEA Annual Report; NEA OECD: Paris, France, 2021; p. 91.
16. Uranium 2016: Resources, Production and Demand; NEA OECD: Paris, France, 2016; 546p.
17. Geological Classification of Uranium Deposits and Description of Selected Examples; IAE: Vienna, Austria, 2018; 417p.
18. World Uranium Geology, Exploration, Resources and Production; IAEA: Vienna, Austria, 2020; 972p.
19. Brookins, D.G. Geochemical Aspects of Radioactive Waste Disposal; Springer: New York, NY, USA, 1984; 347p.
20. Plutonium Separation in Nuclear Power Programs. Status, Problems, and Prospects of Civilian Reprocessing Around th e World; Princeton University: Princeton, NJ, USA, 2015; p. 182.
21. Ojovan, M.I.; Lee, W.E.; Kalmykov, S.N. An Introduction to Nuclear Waste Immobilization, 3rd ed.; Elsevier: Amsterda m, The Netherlands, 2019; p. 497.
22. Ewing, R.C. Actinides and radiation effects: Impact on the back-end of the nuclear fuel cycle. Mineral. Mag. 2011, 75, 2 359–2377.
23. Gumber, N.; Pai, R.V.; Phatak, R.; Adiraju, B.; Sahu, M.; Jagannath, J.; Sudarshan, K. Synthesis, characterization and crystal chemistry of uranium and cerium doped yttrium titanate pyrochlore: A potential waste immobilization matrix. J. N ucl. Mater. 2021, 556, 153191.
24. Zhang, K.; Luo, B.; Zhang, H. Immobilization of CeO2 using single-phase zirconolite and the chemical stability analysis. Mater. Res. Express 2019, 6, 115526.
25. Zhang, S.; Xu, B.; Cheng, J.; Luo, S.; Ding, Y.; Ji, S.; Duan, T.; Ma, J.; Jiang, C. Phase evolution and chemical stability of Nd-doped Y3Fe5O12 waste forms synthesized in molten salt at a low temperature. J. Am. Ceram. Soc. 2021, 105, 1 459–1471.
26. Shannon, R.D. Revised effective ionic radii and systematic studies of interatomic distances in halides and chalcogenide s. Acta Crystallogr. Sect. A 1976, 32, 751–767.
27. Zhang, Y.; Kong, L.; Ionescu, M.; Gregg, D.J. Current advances on titanate glass-ceramic composite materials as wast e forms for actinide immobilization: A technical review. J. Eur. Ceram. Soc. 2022, 42, 1852–1876.
28. Ringwood, A.E.; Kesson, S.E.; Ware, N.G.; Hibberson, W.O.; Major, A. The SYNROC process: A geochemical approac h to nuclear waste immobilization. Geochem. J. 1979, 13, 141–169.

29. Ringwood, A.E.; Kesson, S.E.; Ware, N.G.; Hibberson, W.O.; Major, A. Immobilisation of high-level nuclear reactor wast es in SYNROC. Nature 1979, 278, 219–223.

30. Ringwood, A.E.; Kesson, S.E.; Reeve, K.D.; Levins, D.M.; Ramm, E.J. Synroc. In Radioactive Waste Forms for the Fut ure; Lutze, W., Ewing, R.C., Eds.; Elsevier: New York, NY, USA, 1988; pp. 233–334.

31. Laverov, N.P.; Omel'yanenko, B.I.; Yudintsev, S.V.; Nikonov, B.S. Zirconolite as a matrix for immobilization of high-level radioactive wastes (HLW). Geol. Ore Depos. 1996, 38, 345–352.

32. Advocat, T.; Fillet, C.; Marillet, J.; Boubals, J.M.; Bonnetier, A. Nd-doped zirconolite ceramic and glass ceramic synthesi zed by melting and controlled cooling. Mat. Res. Soc. Symp. Proc. 1998, 506, 55–61.

33. Advocat, T.; McGlinn, P.J.; Fillet, C.; Leturcq, G.; Schuller, S.; Bonnetier, A.; Hart, K. Melted synthetic zirconolite-based matrices: Effect of cooling rate and heat treatment on ceramic microstructure and chemical durability. Mat. Res. Soc. S ymp. Proc. 2001, 663, 277–284.

34. Xu, H.; Wang, Y. Crystallization sequence and microstructure evolution of Synroc samples crystallized from CaZrTi2O7 melts. J. Nucl. Mater. 2000, 279, 100–106.

35. Vance, E.R.; Lumpkin, G.R.; Carter, M.L.; Cassidy, D.J.; Ball, C.J.; Day, R.A.; Begg, B.D. Incorporation of Uranium in Zi rconolite (CaZrTi2O7). J. Am. Ceram. Soc. 2002, 85, 1853–1859.

36. Loiseau, P.; Caurant, D.; Baffier, N.; Mazerolles, L.; Fillet, C. Glass–ceramic nuclear waste forms obtained from SiO2–A l2O3–CaO–ZrO2–TiO2 glasses containing lanthanides (Ce, Nd, Eu, Gd, Yb) and actinides (Th): Study of internal crysta llization. J. Nucl. Mater. 2004, 335, 14–32.

37. Vance, E.R.; Moricca, S.; Begg, B.D.; Stewart, M.W.A.; Zhang, Y.; Carter, M.L. Advantages hot isostatically pressed cer amic and glass-ceramic waste forms bring to the immobilization of challenging intermediate- and high-level nuclear was tes. Adv. Sci. Technol. 2010, 73, 130–135.

38. Stefanovsky, S.V.; Chizhevskaya, S.V.; Mironov, A.S.; Kiryanova, O.I.; Yudintsev, S.V. Synthetic calcium-free REE-subs tituted zirconolites. Perspekt. Mater. 2003, 6, 61–68. (In Russian)

39. Strachan, D.M.; Scheele, R.D.; Buck, E.C.; Kozelisky, A.E.; Sell, R.L.; Elovich, R.J.; Buchmiller, W.C. Radiation damag e effects in candidate titanates for Pu disposition: Zirconolite. J. Nucl. Mater. 2008, 372, 16–31.

40. Yin, D.; Zhang, K.; Peng, L.; He, Z.; Liu, Y.; Zhang, H.; Lu, X. Solid-state reaction synthesis and chemical stability studi es in Nd-doped zirconolite-rich ceramics. J. Rare Earths. 2018, 36, 492–498.

41. Zhang, K.; Yin, D.; Lu, X.; Zhang, H. Self-propagating high-temperature synthesis, phase composition and aqueous dur ability of Nd–Al bearing zirconolite-rich composites as nuclear waste form. Adv. Appl. Ceram. 2018, 117, 78–84.

42. Blackburn, L.R.; Gardner, L.J.; Sun, S.K.; Maddrell, E.R.; Stennett, M.C.; Corkhill, C.L.; Hyatt, N.C. Hot Isostatically Pre ssed Zirconolite Wasteforms for Actinide Immobilisation. IOP Conf. Ser. Mater. Sci. Eng. 2020, 818, 012010.

43. Gregg, D.J.; Farzana, R.; Dayal, P.; Holmes, R.; Triani, G. Synroc technology: Perspectives and current status (Revie w). J. Am. Ceram. Soc. 2020, 103, 5424–5441.

44. Zhu, H.; Wang, F.; Liao, Q.; Zhu, Y. Synthesis and characterization of zirconolite—sodium borosilicate glass-ceramics f or nuclear waste immobilization. J. Nucl. Mater. 2020, 532, 152026.

45. Zhu, H.; Wang, F.; Liao, Q.; Wang, Y.; Zhu, Y. Effect of CeO2 and Nd2O3 on phases, microstructure and aqueous chem ical durability of borosilicate glass-ceramics for nuclear waste immobilization. Mater. Chem. Phys. 2020, 249, 122936.

46. Caurant, D.; Majérus, O. Glasses and Glass-Ceramics for Nuclear Waste Immobilization. In Encyclopedia of Materials: Technical Ceramics and Glasses; Pomeroy, M., Ed.; Elsevier: Oxford, UK, 2021; Volume 2, pp. 762–790.

47. Aldean, I.; Sun, S.-K.; Wilkins, M.C.D.; Gardner, L.J.; Mason, A.R.; Stennett, M.C.; Corkhill, C.L.; Hyatt, N.C.; Blackbur n, L.R. Synthesis and characterisation of Ce-doped zirconolite Ca0.80Ce0.20ZrTi1.60M0.40O7 (M = Fe, Al) formed by r eactive spark plasma sintering (RSPS). Mat. Res. Soc. Adv. 2022, 7, 75–80.

48. Dayal, P.; Farzana, R.; Zhang, Y.; Lumpkin, G.R.; Holmes, R.; Triani, G.; Gregg, D.J. Profiling hot isostatically pressed c anister–wasteform interaction for Pu-bearing zirconolite-rich wasteforms. J. Am. Ceram. Soc. 2022, 105, 1–14.

49. Lumpkin, G.R. Alpha-decay damage and aqueous durability of actinide host phases in natural systems. J. Nucl. Mater. 2001, 289, 136–166.

50. Lumpkin, G.R.; Geisler-Wierwille, T. Minerals and Natural Analogues. In Comprehensive Nuclear Materials; Konings, R., Allen, T., Stoller, R., Yamanak, S., Eds.; Elsevier: Amsterdam, The Netherlands, 2012; pp. 563–600.

51. Lumpkin, G.R. Ceramic Host Phases for Nuclear Waste Remediation. In Experimental and Theoretical Approaches to A ctinide Chemistry; Gibson, J.K., de Jong, W.A., Eds.; Wiley & Sons Ltd.: Hoboken, NJ, USA, 2018; pp. 333–377.

52. Omel’yanenko, B.I.; Livshits, T.S.; Yudintsev, S.V.; Nikonov, B.S. Natural and artificial minerals as matrices for immobiliz ation of actinides. Geol. Ore Depos. 2007, 49, 173–193.

53. Williams, C.T.; Giere, R. Zirconolite: A Review of localities worldwide, and a compilation of its chemical compositions. B ull. Nat. Hist. Mus. Lond. 1996, 52, 1–24.

54. Hudson Institute of Mineralogy. mindat.org. Zirconolite. Available online: https://www.mindat.org/min-4422.html) (access ed on 6 July 2022).

55. Bayliss, P.; Mazzi, F.; Munno, R.; White, T.J. Mineral nomenclature: Zirconolite. Mineral. Mag. 1989, 53, 565–569.

56. Ventura, G.D.; Bellatreccia, F.; Williams, T. Zirconolite with significant REEZrNb(Mn,Fe)O7 from a xenolith of the Laach er see eruptive center, Eifel volcanic region, Germany. The Canad. Mineral. 2000, 38, 57–65.

57. Zubkova, N.V.; Chukanov, N.V.; Pekov, I.V.; Ternes, B.; Schüller, W.; Ksenofontov, D.A.; Pushcharovsky, D.Y. The cryst al structure of nonmetamict Nb-rich zirconolite-3T from the Eifel paleovolcanic region, Germany. Z. Krist. 2018, 233, 46 3–468.

58. Ringwood, A.E. Disposal of high-level nuclear wastes: A geological perspective. Mineral. Mag. 1985, 49, 159–176.

59. Fielding, P.E.; White, T.J. Crystal chemical incorporation of high-level waste species in aluminotitanate-based ceramics: Valence, location, radiation damage, and hydrothermal durability. J. Mater. Res. 1987, 2, 387–414.

60. Kesson, S.E.; Sinclair, W.J.; Ringwood, A.E. Solid solution limits in Synroc zirconolite. Nucl. Chem. Waste Managem. 1 983, 4, 259–265.

61. Coelho, A.A.; Cheary, R.W.; Smith, K.L. Analysis and structural determination of Nd-substituted zirconolite-4M. J. Solid State Chem. 1997, 129, 346–359.

62. Caurant, D.; Loiseau, P.; Bardez, I. Structural characterization of Nd-doped Hf-zirconolite Ca1−xNdxHfTi2−xAlxO7 cera mics. J. Nucl. Mater. 2010, 407, 88–99.

63. Mazzi, F.; Munno, R. Calciobetafite (new mineral of the pyrochlore group) and related minerals from Campi Flegrei, Ital y; crystal structures of polymignyte and zirkelite: Comparison with pyrochlore and zirconolite. Am. Mineral. 1983, 68, 26 2–276.

64. White, T.J. The microstructure and microchemistry of synthetic zirconolite, zirkelite and related phases. Am. Mineral. 19 84, 69, 1156–1172.

65. Smith, K.L.; Lumpkin, G.R. Structural features of zirconolite, hollandite and perovskite, the major waste-bearing phases in Synroc. In Defects and Processes in the Solid State: Geoscience Applications; Boland, J.N., Fitzgerald, J.D., Eds.; El sevier: Amsterdam, The Netherlands, 1993; pp. 401–422.

66. Blackburn, L.R.; Sun, S.-K.; Gardner, L.J.; Maddrell, E.R.; Stennett, M.C.; Corkhill, C.L.; Hyatt, N.C. Synthesis, structur e, and characterization of the thorium zirconolite CaZr1−xThxTi2O7 system. J. Am. Ceram. Soc. 2021, 104, 2937–295 1.

67. Gilbert, M.R.; Selfslag, C.; Walter, M.; Stennett, M.C.; Somers, J.; Hyatt, N.C.; Livens, F.R. Synthesis and characterisati on of Pu-doped zirconolites—(Ca1−xPux)Zr(Ti2−2xFe2x)O7. IOP Conf. Ser. Mater. Sci. Eng. 2009, 9, 012007.

68. Grey, I.E.; Mumme, W.G.; Ness, T.J.; Roth, R.S.; Smith, K.L. Structural relations between weberite and zirconolite polyt ypes—Refinements of doped 3T and 4M Ca2Ta2O7 and 3T CaZrTi2O7. J. Solid State Chem. 2003, 174, 285–295.

69. Kong, L.; Karatchevtseva, I.; Zhang, Y.; Wei, T. The incorporation of Nd or Ce in CaZrTi2O7 zirconolite: Ceramic versus glass-ceramic. J. Nucl. Mater. 2021, 543, 152583.

70. Gin, S.; Jollivet, P.; Tribet, M.; Peuget, S.; Schuller, S. Radionuclides containment in nuclear glasses: An overview. Radi ochimica Acta. 2017, 105, 927–959.

71. Cachia, J.-N.; Deschanels, X.; Auwer, C.D.; Pinet, O.; Phalippou, J.; Hennig, C.; Scheinost, A. Enhancing cerium and pl utonium solubility by reduction in borosilicate glass. J. Nucl. Mater 2006, 352, 182–189.

72. Caurant, D.; Majerus, O.; Loiseau, P.; Bardez, I.; Baffier, N.; Dussossoy, J.L. Crystallization of neodymium-rich phases i n silicate glasses developed for nuclear waste immobilization. J. Nucl. Mater. 2006, 354, 143–162.

73. McCloy, J.S.; Schuller, S. Vitrification of wastes: From unwanted to controlled crystallization, a review. Comptes Rendu s. Géoscience 2022, 354, 1–40.

74. Blackburn, L.R.; Bailey, D.J.; Sun, S.-K.; Gardner, L.J.; Stennett, M.C.; Corkhill, C.L.; Hyatt, N.C. Review of zirconolite c rystal chemistry and aqueous durability. Adv. Appl. Ceram. 2021, 120, 69–83.

75. Blackburn, L.R.; Sun, S.; Gardner, L.J.; Maddrell, E.R.; Stennet, M.C.; Hyatt, N.C. A systematic investigation of the pha se assemblage and microstructure of the zirconolite CaZr1−xCexTi2O7. J. Nucl. Mater. 2020, 535, 152137.

76. Ji, S.; Su, M.; Liao, C.; Ma, S.; Wang, Z.; Shih, K.; Chang, C.-K.; Lee, J.-F.; Chan, T.-S.; Li, Y. Synchrotron x-ray spectroscopy investigation of the Ca1−xLnxZrTi2−x(Al,Fe)xO7 zirconolite ceramics (Ln = La, Nd, Gd, Ho, Yb). J. Am. Ceram. Soc. 2020, 103, 1463–1475.

77. Maddrell, E.R.; Paterson, H.C.; May, S.E.; Burns, K.M. Phase evolution in zirconolite glass-ceramic wasteforms. J. Nucl. Mater. 2017, 423, 380–387.

78. Vance, E.R.; Agraval, D.K. Incorporation of radionuclides in crystalline titanates. Nucl. Chem. Waste Managem. 1982, 3, 229–234.

79. Weber, W.J.; Ewing, R.C.; Catlow, C.R.A. Radiation effects in crystalline ceramics for the immobilization of high-level nuclear waste and plutonium. J. Mat. Res. 1998, 13, 1434–1479.

80. Zhang, Y.; Stewart, M.W.A.; Li, H.; Carter, M.L.; Vance, E.R.; Moricca, S. Zirconolite-rich titanate ceramics for immobilisation of actinides—Waste form/HIP can interactions and chemical durability. J. Nucl. Mater. 2009, 395, 69–74.

81. Amoroso, J.; Marra, J.C.; Tang, M.; Lin, Y.; Chen, F.; Su, D.; Brinkman, K.S. Melt processed multiphase ceramic waste forms for nuclear waste immobilization. J. Nucl. Mater. 2014, 454, 12–21.

82. Leturcq, G.; McGlinn, P.J.; Barbe, C.; Blackford, M.G.; Finnie, K.S. Aqueous alteration of nearly pure Nd-doped zirconolite (Ca0.8Nd0.2ZrTi1.8Al0.2O7), a passivating layer control. Appl. Geochem. 2005, 20, 899–906.

83. Pöml, P.; Geisler, T.; Cobos-Sabaté, J.; Wiss, T.; Raison, P.E.; Schmid-Beurmann, P.; Deschanels, X.; Jégou, C.; Heimink, J.; Putnis, A. The mechanism of the hydrothermal alteration of cerium- and plutonium-doped zirconolite. J. Nucl. Mater. 2011, 410, 10–23.

84. Jafar, M.; Sengupta, P.; Achary, S.N.; Tyagi, A.K. Phase evolution and microstructural studies in CaZrTi2O7 (zirconolite)—Sm2Ti2O7 (pyrochlore) system. J. Eur. Ceram. Soc. 2014, 34, 4373–4381.

85. Malmström, J.; Reusser, E.; Gieré, R.; Lumpkin, G.R.; Düggelin, M.; Mathys, D.; Guggenheim, R. Zirconolite corrosion in dulite acidic and basic fluids at 180–700 °C and 50 MPa. Mat. Res. Soc. Symp. Proc. 1999, 556, 165–172.

86. Malmstrom, J.; Reusser, E.; Giere, R.; Lumpkin, G.R.; Blackford, M.G.; Duggelin, M.; Mathys, D.; Guggenheim, R.; Gunther, D. Formation of perovskite and calzirtite during zirconolite alteration. Mat. Res. Soc. Symp. Proc. 2000, 608, 475–480.

87. Bakel, A.J.; Mertz, C.J.; Hash, M.C.; Chamberlain, D.B. The long-term corrosion behavior of titanate ceramics for Pu disposition: Rate-controlling processes. Mat. Res. Soc. Symp. Proc. 2000, 608, 387–392.

88. Gieré, R.; Malmström, J.; Reusser, E.; Lumpkin, G.R.; Düggelin, M.; Mathys, D.; Guggenheim, R.; Günther, D. Durability of zirconolite in hydrothermal fluids: Implications for nuclear waste disposal. Mat. Res. Soc. Symp. Proc. 2001, 663, 267–276.

89. Morgan, P.E.D.; Ryerson, F.J. A new “cubic” crystal compound. J. Mater. Sci. Lett. 1982, 1, 351–352.

90. Laverov, N.P.; Urusov, V.S.; Krivovichev, S.V.; Pakhomova, A.S.; Stefanovsky, S.V.; Yudintsev, S.V. Modular nature of the polysomatic pyrochlore–murataite series. Geol. Ore Depos. 2011, 53, 273–294.

91. Laverov, N.P.; Yudintsev, S.V.; Stefanovskii, S.V.; Omel’yanenko, B.I.; Nikonov, B.S. Murataite Matrices for Actinide Wastes. Radiochemistry 2011, 53, 229–243.

92. Laverov, N.P.; Yudintsev, S.V.; Stefanovsky, S.V.; Omel’yanenko, B.I.; Nikonov, B.S. Murataite as a universal matrix for immobilization of actinides. Geol. Ore Depos. 2006, 48, 335–356.

93. Laverov, N.P.; Omel’yanenko, B.I.; Yudintsev, S.V.; Nikonov, B.S.; Sobolev, I.A.; Stefanovsky, S.V. Mineralogy and geochemistry of matrices for the immobilization of high-level radioactive wastes. Geol. Ore Deposits. 1997, 39, 179–193.

94. Yudintsev, S.V.; Danilov, S.S.; Vinokurov, S.E.; Stefanovskaya, O.I.; Nikonov, B.S.; Nikol’sky, M.S.; Skvortsov, M.V.; Myasoedov, B.F. Phase composition and hydrothermal stability of ceramics based on murataite. Radiochemistry 2020, 62, 744–751.

95. Pakhomova, A.S.; Krivovichev, S.V.; Yudintsev, S.V.; Stefanovsky, S.V. Polysomatism and structural complexity: Structure model for murataite-8C, a complex crystalline matrix for the immobilization of high-level radioactive waste. Eur. J. Mineral. 2016, 28, 205–214.

96. Pakhomova, A.S.; Krivovichev, S.V.; Yudintsev, S.V.; Stefanovsky, S.V. Synthetic murataite-3C, a complex form for long-term immobilization of nuclear waste: Crystal structure and its comparison with natural analogues. Z. Krist. Cryst. Mater. 2013, 228, 151–156.

97. Krivovichev, S.V.; Yudintsev, S.V.; Stefanovsky, S.V.; Organova, N.I.; Karimova, O.V.; Urusov, V.S. Murataite–pyrochlore series: A family of complex oxides with nanoscale pyrochlore clusters. Angew. Chem. 2010, 122, 10178–10180.

98. Krivovichev, S.; Yudintsev, S.; Pakhomova, A.; Stefanovsky, S. Murataite-Pyrochlore Ceramics as Complex Matrices for Radioactive Waste Immobilization: Structural and Microstructural Mechanisms of Crystallization. In International Congr

ess on Applied Mineralogy; Springer: Cham, Switzerland, 2019; pp. 447–450.

99. Yudintsev, S.; Stefanovsky, S.; Nikonov, B.; Stefanovsky, O.; Nickolskii, M.; Skvortsov, M. Phase formation at synthesis of murataite-crichtonite ceramics. J. Nucl. Mater. 2019, 517, 371–379.
100. Nickolsky, M.S.; Yudintsev, S.V. Electron backscattered diffraction for the study of matrices for immobilization of actinides composed of the murataite-type phases. Crystallogr. Rep. 2021, 66, 130–141.
101. Yudintsev, S.V.; Nickolsky, M.S.; Nikonov, B.S. Study of Matrices for Immobilization of 99Tc by the EBSD Method. Dokl. Earth Sci. 2021, 500, 794–801.